PCCP

ROYAL SOCIETY OF CHEMISTRY

PAPER

View Article Online
View Journal

Cite this: DOI: 10.1039/d1cp01716k

Unveiling the mechanisms behind the ferroelectric response in the Sr(Nb,Ta)O_2N oxynitrides

J. S. Gelves-Badillo, [a] Aldo H. Romero [bc] and A. C. Garcia-Castro *[a]

Received 21st April 2021,
Accepted 21st June 2021

DOI: 10.1039/d1cp01716k

rsc.li/pccp

Oxynitride perovskites of the type ABO_2N have attracted considerable attention thanks to their potential ferroelectric behavior and tunable bandgap energy, making them ideal candidates for photocatalysis processes. Therefore, in order to shed light on the origin of their ferroelectric response, here we report a complete analysis of the structural and vibrational properties of $SrNbO_2N$ and $SrTaO_2N$ oxynitrides. By employing first-principles calculations, we analyzed the symmetry in-equivalent structures considering the experimentally reported parent *I*4/*mcm* space group (with a phase $a^0a^0c^-$ in Glazer's notation). Based on the *I*4/*mcm* reference within the 20-atoms unit-cell, we found and studied the ensemble of structures where different octahedral anionic orderings are allowed by symmetry. Thus, by exploring the vibrational landscape of the *cis*- and *trans*-type configuration structures and supported by the ionic eigendisplacements and the Born effective charges, we explained the mechanism responsible for the appearance of stable ferroelectric phases in both anionic orderings. The latter goes from covalent-driven in the *trans*-type ordering to the geometrically-driven in the *cis*-type configuration. Finally, we found in both cases that the biaxial *xy* epitaxial strain considerably enhances such ferroelectric response.

1 Introduction

In the last two decades, theoretical and experimental techniques associated with the analysis of multifunctional polar materials have developed exponentially.[1] In particular, multiferroics and ferroelectrics, based on perovskite-like oxides, have been in the center of discussion thanks to their recognized features in piezoelectricity, magnetoelectricity, and polar response, mainly driven by the reported magnetic and ferroelectric features.[2,3] Unfortunately, the ferroelectric's operation temperature enhancement, aiming to reach values well above room temperature, and spontaneous polarization's intensity are still functionalities in pursuit in the field. Moreover, enhanced ferroelectrics can drive to tangible advances in non-volatile ferroelectric-based transistors[4] and provide better performance in the photocatalysis mechanisms intrinsic to the water-splitting process.[5–8] Here, perovskite-like oxide materials dominate the interest of most research groups.

The replacement of A- and B-sites, in materials with stoichiometries ABO_3 and A_2BO_4, is highlighted as the preferred route to enhance ferroelectric performance.[9] To date, few proposals based on the exploration of the anionic X-site, such as fluorine,[10–14] sulphur,[15] and nitrogen[16–19] have shown promising results. It has recently been demonstrated that heteroanionic compounds are good multifunctional candidates, especially for ferroelectric applications.[20,21] In this arena, oxynitrides (*i.e.* $ABO_{3-x}N_x$) are in the spotlight thanks to their capability of absorbing light in the visible region. This property makes them ideal candidates in photocatalysis applications by proper tuning of the bandgap with variations of the O/N ratio, which lead to different octahedral occupation.[22] These anionic substitutions are described by the nitrogen's and oxygen's occupation and coordination in the B-centered octahedra. As a result, different anionic orderings are obtained as the *cis*-, *trans*-, *fac*-, and *mer*-type, shown in Fig. 1a. For instance, such anionic orderings are strongly correlated to the electronic and structural properties of oxynitrides.

Regarding the polar response, the ferroelectric behavior has been measured in several oxynitride compounds in which a successful synthesis of epitaxial thin films has been obtained.[23,24] Moreover, the ability to tune their electronic structure, thanks to their O/N anion-substitution, has been highlighted.[25] The B-site off-centering in the $B(O/N)_6$ octahedra is probably the source of the reported polar response, and it could be the main reason for the ferroelectric behavior. Unfortunately, the latter explanation depends on the *trans*-type configuration despite the *cis*-type being the ground state. This anionic order preference is explained in terms of maximizing the B:d–N:p bonding strength that lowers the *cis*-type energy compared to the *trans*-type anionic configuration's energy. For

[a] School of Physics, Universidad Industrial de Santander, Carrera 27 Calle 09, 680002, Bucaramanga, Colombia. E-mail: acgarcia@uis.edu.co
[b] Department of Physics and Astronomy, West Virginia University, Morgantown, WV 26506-6315, USA. E-mail: Aldo.Romero@mail.wvu.edu
[c] Facultad de Ingeniería-BUAP, Apartado Postal J-39, Puebla, Pue. 72570, Mexico

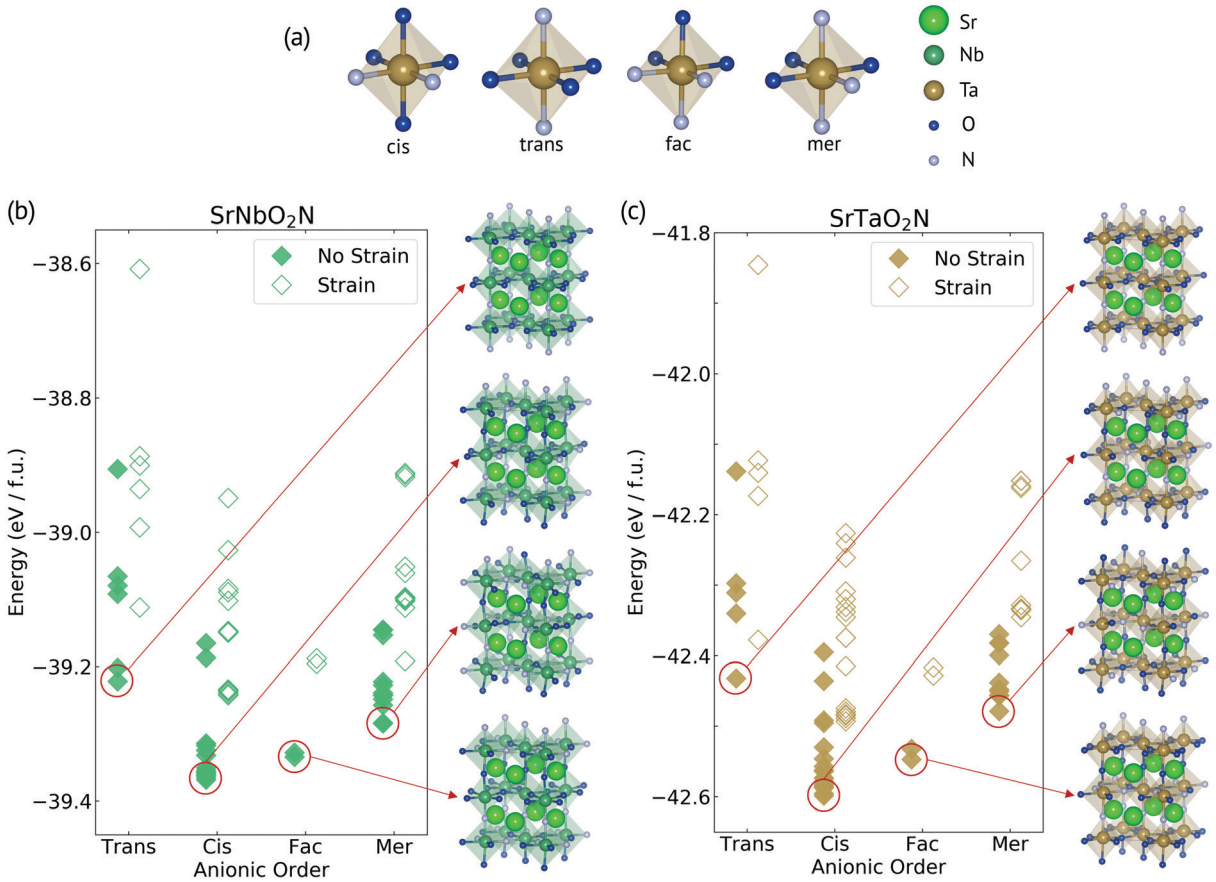

Fig. 1 Panel (a) shows the *cis*, *trans*, *fac*, and *mer* anionic orderings within the (Nb,Ta)$O_{6-x}N_x$ octahedra. Oxygen and nitrogen sites are displayed in blue and grey colors, respectively, whereas niobium, tantalum, and strontium are shown in dark green, orange, and light green as denoted. The total energies and structures, computed based on the symmetry occupation disorder methodology, are presented for the $SrNbO_2N$ and $SrTaO_2N$ at (b) and (c) panels. Additionally, the lowest energy configurations for each anionic ordering are also shown in (b) and (c).

example, although the ferroelectric response was observed in the $SrTaO_2N$ oxynitride,[23] the *cis*-type anion order was identified as the ground state in which the ferroelectric's origin and switching mechanism are still unknown. In conclusion, whereas the polar and ferroelectric response in this type of oxynitrides has been experimentally demonstrated,[23,26–30] a more profound theoretical explanation and understanding of its physical origin is still to pursue. This paper aims to shed light on the physical mechanisms that give rise to the observed polar and ferroelectric behavior in $SrNbO_2N$ (SNON) and $SrTaO_2N$ (STON) as prototype oxynitrides. We explore the structural and vibrational landscapes in these oxynitrides and investigate the polar and ferroelectric response reasons based on first-principles calculations. Section 2 describes the computational details of our calculations. Section 3 presents our results and offers a discussion of the physical meaning of the calculated quantities. We finalize the paper by concluding and making suggestions for further studies.

2 Computational details

We employed density-functional theory (DFT)[31,32] calculations as implemented in the vasp code (version 5.4.4).[33,34] The projected-augmented waves, PAW,[35] approach was used to represent the valence and core electrons. The electronic configurations considered in the pseudo-potentials for the calculations were Sr: ($4s^2 4p^6 5s^2$, version 07Sep2000), Nb: ($4p^6 4d^3 5s^2$, version 08Apr2002), Ta: ($5p^6 5d^3 6s^2$, version 07Sep2000), O: ($2s^2 2p^4$, version 08Apr2002), and N: ($2s^2 2p^3$, version 08Apr2002). The exchange–correlation was represented within the generalized gradient approximation GGA-PBEsol parametrization[36] and the d-electrons were corrected through the DFT+U approximation within the Liechtenstein formalism[37] using a U = 4.0 eV for Nb and Ta. This U value was included to correct the electronic correlation misrepresentation at the Nb:4d and Ta:5d orbitals induced by the different anionic orderings and, consequently, partial d-occupation. The periodic solution of the crystal was represented by using Bloch states with a Monkhorst–Pack[38] k-point mesh of 8 × 8 × 6 and 600 eV energy cut-off to give forces convergence within the error smaller than 0.001 eV $Å^{-1}$. Born effective charges and phonon calculations were performed within the density functional perturbation theory (DFPT)[39] as implemented in the vasp code. Phonon-dispersions were post-processed in the Phonopy code.[40] The atomic structure figures were elaborated with the support of the VESTA code.[41] Spontaneous polarization was

computed using the Berry-phase approach.[42] Finally, to treat different O and N concentrations and anionic orderings, we employed the site-occupation disorder approach as implemented in the SOD package.[43] In this package, all in-equivalent configurations of site substitutions are constructed with a predefined supercell size based on an initial target unit cell.

3 Results and discussion

3.1 Anionic ordering analysis

As a first step in the analysis, we explored the anionic ordering in $SrNbO_2N$ and $SrTaO_2N$. For such, it is essential to consider that O^{2-} and N^{3-} anions can be organized in multiple combinations to occupy the allowed X-sites within the $Sr(Nb,Ta)O_2N$ crystal. The Site-Occupancy Disorder (SOD) method[43] allows us to reduce such a wide range of site-occupancy possibilities to a small set of symmetry-different structures. This procedure is carried out based on the equivalence criteria between two structures, which is defined in terms of the existence of an isometric transformation mapping between configurations.[44] Specifically, this method generates all the possible structures for a specific content ratio of atomic substitutions. Then, using the symmetry operations of the parent structure (*i.e.*, the initial unit cell where the substitutions are performed to build the supercell) as isometric trial transformations, it identifies the equivalent and consequently the symmetrically different structures out of all the site-occupancy possibilities. More details can be found in ref. 43. Following this procedure, we extracted and analyzed the in-equivalent symmetry structures in the 20-atoms cell for the O/N ratio of 2/1.

As a starting symmetry, we used the parent *I*4/*mcm*, which is the experimentally reported long-range structure, in both B = Nb, and Ta[45,46] cases. For this structure, the $a^0a^0c^-$ Glazer's rotation pattern is reported.[47] By following the previously discussed methodology, we obtained 35 symmetry in-equivalent structures that can be indexed as *cis*-, *trans*-, *mer*-, and *fac*-type anionic orderings[20,48,49] and shown in Fig. 1b and c. *fac*- and *mer*-type orderings are composed of a combination of the basic *cis*- and *trans*-type arrangements. Then, the selected in-equivalent structures are electronically and geometrically relaxed. The structures' energies are compared and used to arrange those from the most energetically stable to the least. Additionally, considering that most of the experimental reports on the ferroelectric and polar behavior in these oxynitrides are in the form of thin films, we also considered the epitaxial compression strain in the *xy*-plane induced by the $SrTiO_3$ substrate. Interestingly, the biaxial strain has been widely used to tune and enhance the ferroelectric properties in similar compounds.[50–52] Consequently, we included in our analysis the epitaxial strain effect by constraining the *xy*-plane to the $SrTiO_3$ experimentally reported lattice parameter (*i.e.* a = 3.905 Å). Fig. 1b and c shows the total energy per formula unit (*i.e.* f.u.) after full structural relaxation, for $SrNbO_2N$ and $SrTaO_2N$ oxynitrides, respectively. In the same figure, we also include the total energies obtained under the *xy*-plane epitaxial strain effect. Our calculations show that the *cis*-type octahedral arrangement is the only one present in the lowest energy structure in both oxynitrides. This result is in agreement with previous publications.[48,53,54] Here, the *cis* anionic ordering favors the maximization of the N:p-(Nb,Ta):d hybridization which, in turn, is strengthening the N–(Nb,Ta) bonding.[48,53,54] The *fac*-type configuration is the closest to the *cis* ground state by ordering the structures based on the total energy. This total energy proximity is due to the presence, in the *fac* ordering, of two *cis*-type arrangements in the same octahedra, see Fig. 1a. These groups of structures are followed in energy by the *mer*-type and, finally, the *trans*-type orderings. The *mer*-type can be obtained from two *cis*-type combination orderings, but at the same time, a *trans*-type can also be identified within the same octahedra, as depicted in Fig. 1a. Thus, *fac*- and *mer*-type anionic ordering energies lie in a range defined between the limits of the *cis*- and *trans* anionic ordering. This energy arrangement is summarized in Fig. 1b and c. Regarding the *trans*-type configurations, we found the energy differences to be ΔE = 146.8 meV per f.u. and 166.7 meV per f.u. for SNON and STON, respectively, above the *cis* observed ground state. These total energy differences agree with the reduction of the N:p-(Nb,Ta):d hybridization induced by the *trans* anionic coordination.

In strained oxynitrides, the structures' total energy *versus* the order type follows the same trend as the unstrained cases. Nonetheless, it is essential to mention that the energy difference between the lowest *cis* and *trans* configurations is reduced to 130.4 meV per f.u. in the SNON oxynitride and 115.7 meV per f.u. for the STON case. Such values are lower than the unstrained scenario. This observation suggests that the epitaxial strain imposed by the substrate at the thin film deposition process could increase the probability of observing a more significant concentration of *trans*-type of anionic domains. Interestingly, both *cis*- and *trans*-configurations, have been experimentally suggested to coexist in oxynitrides such as $BaTaO_2N$,[55] $LaTiO_2N$,[56] $SrTaO_2N$,[28] and $SrNbO_2N$.[30] Interestingly, the energy difference between the *cis* and *trans* configurations is smaller than the one observed at, for example, $BaTaO_2N$ ($\Delta E \approx 300$ meV per f.u.).[55] This slight energy difference implies that the *trans*-type oxynitride could be present in both oxynitrides' experimental synthesis when grown in thin-film form. Similarly, less energetically favorable *trans*-type structures, as well as *mer*- and *fac*-type, can be stabilized by biaxial strain control. In essence, we could expect that, although the lowest energy structures exhibit a *cis*-type anionic ordering, the synthesized materials in bulk and thin-films probably show a mixture of configurations and combinations of anionic orderings where the *cis*-type configuration is present with the most considerable contribution into the samples. It is worth noticing that whereas the *cis* and *trans*-type satisfy the local charge neutrality criteria between the Sr cations and the $(Nb,Ta)O_4N_2$ octahedra, the *mer*- and *fac*-types breaks this charge neutrality due to the presence of $(Nb,Ta)O_3N_3$ and $(Nb,Ta)O_5N_1$ octahedra within the 20-atoms *I*4/*mcm* parent unit cell. With this in mind, we analyzed the vibrational landscape of the most fundamental arrangements, *trans*- and *cis*-type, anionic orderings where the local charge neutrality is fulfilled.

This analysis points out the experimentally observed ferroelectric response source, as it is addressed in the following sections.

3.2 *trans*-Type ordering

We computed the phonon-dispersion curves in the equivalent high-symmetry structure where no octahedral rotations are observed within the structure, (*i.e.* $a^0b^0c^0$).[47] The latter vibrational analysis was performed for $SrTaO_2N$ and $SrNbO_2N$, with and without *xy* epitaxial strain's effect. This strategy has been widely applied in oxide and fluorides perovskite-like compounds explaining the mechanisms of the geometrically-driven ferroelectricity,[10,13,57,58] covalent-driven,[59–62] and hybrid improper ferroelectricity in multiple materials.[63,64] As the *trans*-type configuration is considered into the pseudo-cubic perovskite structure with no octahedral rotations, a *P*4/*mmm* phase was identified as the high-symmetry reference. Fig. 2a and b show the phonon-dispersion curves for $SrTaO_2N$ and $SrNbO_2N$, respectively, in the *trans*-type configuration. We observed several unstable modes from this analysis, which we denoted as negative frequency values following the usual convention in phonon spectra analysis. These unstable modes were found at several high-symmetry points along the path (*i.e.* *Γ*–*X*–*M*–*A*–*R*–*Z*) within the Brillouin zone. For instance, we found at the *Γ*-point, an unstable phonon mode associated with a polar Γ_3^- eigendisplacement. On top of this mode, we found other negative modes at the *M*-, *A*-, *R*-symmetry points which are located in the reciprocal coordinates (0.5, 0.5, 0.0), (0.5, 0.5, 0.5), and (0.0, 0.5, 0.5), respectively. These modes are related to in-phase octahedral rotations around the *z*-axis (*i.e.* $a^0b^0c^+$), identified as M_2^+, and out-of-phase modes, identified as A_4^- and A_2 related to the $a^0b^0c^-$ and $a^-a^-c^0$ octahedral rotation patterns, respectively. In Fig. 2c we also present the obtained lowest frequency modes for $SrTaO_2N$ and $SrNbO_2N$ oxynitrides with (denoted as Nb-s and Ta-s) and without (denoted as Nb and Ta) the *xy*-plane STO's epitaxial strain effect. As it can be appreciated, in both Nb and Ta cases, the in-plane strain increases considerably the instabilities which, for example in the SNON case, go from -238 cm^{-1} to -313 cm^{-1} for the polar Γ_3^- mode. Afterward, for the most negative frequency modes, we introduced into the high-symmetry structure the atomic distortions associated to the eigendisplacements of such phonons (*i.e.* modes freezing or condensation). We observed that the A_4^- with a $a^0a^0c^-$ is the lowest energy structure explaining the experimentally observed *I*4/*mcm* ground state. Remarkably, when this structure is analyzed, and the phonon-dispersions computed at the *I*4/*mcm* symmetry, we observed that the Γ_3^- mode remains unstable for both $SrTaO_2N$ and $SrNbO_2N$ oxynitrides with strain, and only in the latter case without this external constraint. This indicating the possible coexistence of octahedral rotations and the Nb-sites polar displacements. Fig. 3a presents the characteristic double-well energy profile obtained after the condensation of the Γ_3^- polar mode in the $a^0a^0c^-$ structure. Here, the structural total energy is computed as a function of the introduction of the atomic displacements related to the Γ_3^- polar mode. Thus, after the

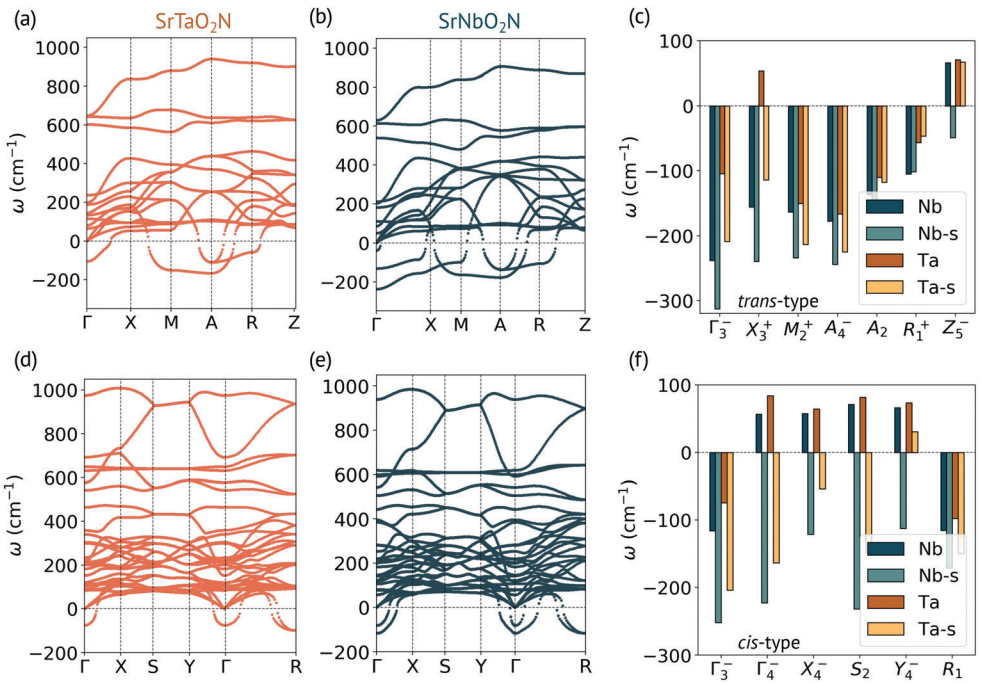

Fig. 2 In (a) and (b) are presented the computed phonon-dispersion curves in the high-symmetry *P*4/*mmm* structure for the *trans*-type configuration in the $SrTaO_2N$ and $SrNbO_2N$ oxynitrides, respectively. In (c) are presented the frequencies for the lower modes, in both $SrTaO_2N$ and $SrNbO_2N$ oxynitrides. In (d) and (e), are shown the phonon-dispersion curves for the *cis*-type anionic order computed in the high-symmetry *Pmma* structure for $SrTaO_2N$ and $SrNbO_2N$, respectively. As in the *trans* case, the corresponding lowest vibrational modes for the *cis*-type ordering are also shown in (f). In both oxynitrides cases, all the unstable modes were computed for SrTaON and $SrNbO_2N$ with (labels Nb-s and Ta-s) and without (labels Nb and Ta) STO's *xy*-biaxial strain effect. Here, the unstable modes are represented as negative frequencies following the usual convention.

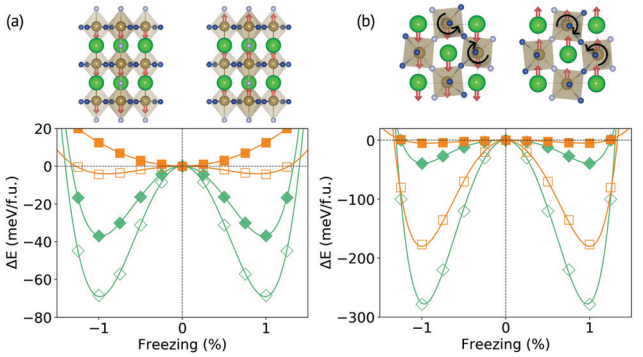

Fig. 3 (a) Condensation of the Γ_3^- mode in the *I*4/*mcm* structure with *trans*-type anionic configuration. The Nb- and Ta-sites off-centering can be observed in the NbO_4N_2 and TaO_4N_2 octahedra. Additionally, the same polar mode condensation is observed in the *Pmma* structure within the *cis*-type configuration (b). Here, the ferroelectric distortion involves a c^+ rotation. In this case, the Nb and Ta contribute and Sr-site to the polar eigendisplacements. $SrNbO_2N$ and $SrTaO_2N$ are shown in green and orange colors, respectively. Filled and empty marks represent the unstrained and strained case, respectively.

mode is fully condensed into the structure, denoted by the energy minima in Fig. 3a, an *I*4*cm* polar ground state is obtained from the *I*4/*mcm* reference structure. In this structure, the Nb- and Ta-sites' off-centering aligned on the *z*-axis can couple with the $a^0a^0c^-$ rotation driving the out-of-plane ferroelectric response in these oxynitrides. In the $SrTaO_2N$ case, we observed a single parabolic energy-well as a function of the polar displacements without epitaxial strain, which suggests a non-polar ground state in this case. This behavior also agrees with the low frequency of the Γ_3^--mode, around -100 cm^{-1}, observed in the high-symmetry *P*4/*mmm* structure. As the strain is imposed, the ferroelectricity is favored in the STON case demonstrated by the energy double-well profile. Moreover, in the SNON case, it can be noted that the ground state is polar even without constraints, and the STO's epitaxial strain enhances it.

As commented above, the eigendisplacements of the Γ_3^--mode lead to an Nb- and Ta-sites off-centering in agreement with a B-site controlled ferroelectricity as observed in similar compounds.[59,65,66] Analyzing the Born-effective charges, Z^*, listed in Table 1, we found large deviations, from their nominal value, of the Nb and Ta's effective charges. Explicitly, the Nb and Ta charges show a difference of 8.3 e^- and 6.3 e^-, respectively, for the Z^*_{zz} component. The previous finding supports the B-site dominated ferroelectricity along the *z*-axis in both oxynitrides[67] which is driven by the strong B:d–X:p covalent bonding. It is important to remark that the tendency to a ferroelectric ground state for the $SrNbO_2N$ oxynitride is not observed for the $SrTaO_2N$ case in the absence of epitaxial strain. This different behavior can be explained in terms of the strength of the metal–anion bond. Since the Ta^{5+} is slightly less electronegative than Nb^{5+}, the Nb–(O,N) covalent interaction tends to be stronger than the Ta–(O,N) one, explaining the preference to the off-centering polar displacement (related to the Γ_3^- unstable phonon mode) for the Nb centered oxynitride. Such more considerable covalent interaction also implies

Table 1 Born-effective charges, Z^* in units of e^-, computed for the *cis*- and *trans*-type configurations at the *Pmma* and *P*4/*mmm* high-symmetry phases respectively. The deviation of the Nb, Ta, O, and N values from their nominal charge suggests the covalent-driven polar character of the possible non-centrosymmetric phases

trans-Type configuration

Site	*xx*	*yy*	*zz*	*xy*	*yx*	Nom.
Sr	2.706	2.706	2.199	0.000	0.000	+2
Nb	8.012	8.012	13.289	0.000	0.000	+5
O	−6.110	−1.733	−2.680	0.000	0.000	−2
N	−2.876	−2.876	−10.129	0.000	0.000	−3
Sr	2.716	2.716	2.229	0.000	0.000	+2
Ta	7.236	7.236	11.276	0.000	0.000	+5
O	−5.593	−1.699	−2.548	0.000	0.000	−2
N	−2.660	−2.660	−8.408	0.000	0.000	−3

cis-Type configuration

Site	*xx*	*yy*	*zz*	*xy*	*xz*	Nom.
Sr	2.566	2.375	2.663	0.000	0.000	+2
Nb	8.255	10.718	7.168	0.000	0.000	+5
O_1	−2.093	−2.019	−5.772	0.000	0.000	−2
O_2	−4.635	−3.605	−2.111	2.161	1.180	−2
N	−4.093	−7.469	−1.947	2.157	4.298	−3
Sr	2.541	2.413	2.685	0.000	0.000	+2
Ta	7.711	9.283	6.684	0.000	0.000	+5
O_1	−2.032	−1.962	−5.333	0.000	0.000	−2
O_2	−4.327	−3.437	−2.029	1.880	1.158	−2
N	−3.893	−6.296	−2.007	1.852	3.264	−3

a tighter repulsion between electronic clouds, which leads to higher instabilities in the vibrational landscape of the $SrNbO_2N$ compared to the $SrTaO_2N$ oxynitride, as shown in Fig. 2. This phenomenon has also been reported in $KNbO_3$ and $KTaO_3$.[68]

Finally, we have estimated the ferroelectric spontaneous polarization value for both, Nb and Ta centered strained oxynitrides. We found rather large values of P_s = 41.6 μC cm^{-2} and 24.1 μC cm^{-2} for $SrNbO_2N$ and $SrTaO_2N$ respectively, under STO's epitaxial strain. In the $SrNbO_2N$ case without strain, we observed a polarization value of P_s = 22.7 μC cm^{-2}. No polarization value is observed for the $SrTaO_2N$ case without strain because, as explained in the discussion above, the ferroelectric *I*4*cm trans*-type structure is unfavorable without STO's strain in this system.

3.3 *cis*-Type ordering

In the *cis*-type anionic ordering, we identified the *Pmma* phase as the high-symmetry structure reference after the geometrical relaxation (*i.e.* inner coordinates and cell parameters). In this phase, no rotations are considered, which corresponds to an $a^0b^0c^0$ octahedral rotation pattern. The phonon-dispersion curves were also computed along the entire high-symmetry path (*i.e.*, *Γ*–*X*–*S*–*Y*–*Γ*–*R*) as depicted in Fig. 2d and e. As it can be appreciated, the R_1 phonon mode is unstable, and it is associated with the $a^0b^+c^0$ rotation around the *y*-axis. Additionally, as in the *trans* ordering case, the polar Γ_3^- is also unstable in the high-symmetry structure. In contrast to the *trans*-ordering, we found that the eigendisplacements of these modes show a polar behavior that involves an $a^0b^0c^+$ octahedral rotation coupled to the Sr and (Nb,Ta)-sites displacements along the *y*-axis.

After identifying the unstable modes, we proceeded with the eigendisplacements condensation within the high-symmetry structure reference. We observed that the Γ_3^- mode drives the structure from the *Pmma* to the $Pmc2_1$ ferroelectric structure. Additionally, after condensing the *R*-mode into the *Pmma* phase, the *C*2/*m* structure was also observed. Remarkably, despite that the polar structure is stable, as shown in Fig. 3b, when extracting the total energy, we observed that the ground state corresponds to the non-polar *C*2/*m* structure. This energy analysis suggests that this structure corresponds to a metastable polar structure higher in energy by 19 meV per f.u. and 20 meV per f.u. for the SNON and STON cases, respectively. Unfortunately, the Γ_3^- and *R*-mode combination is not allowed, and once the polar eigendisplacements are frozen into the *C*2/*m* structure, such polar distortion is removed after the complete geometrical relaxation. Therefore, we conclude that, in the unconstrained and fully relaxed case, the *cis*-type $SrNbO_2N$ and $SrTaO_2N$ oxynitrides ground state belongs to a non-polar structure. As such, the nature of these ground-state phases is mainly due to their anionic ordering and octahedral rotations. Nonetheless, as soon as the STO's strain is applied, several negative modes are also observed induced by the biaxial constraint imposed by the STO substrate, as seen in Fig. 2f. Remarkably, a Γ_4^- mode also appears in the phonon-dispersion curves, suggesting another favorable polar structure. The latter mode leads to an out-of-plane polarization in a *Pma*2 structure after applying the full mode condensation to the high-symmetry reference structure. Surprisingly, the Γ_3^- becomes more unstable thanks to the in-plane biaxial strain, suggesting a tighter competition between the *C*2/*m* and $Pmc2_1$ phases. When analyzing the energy difference between the mentioned phases, now under the epitaxial in-plane strain, we observed that the polar symmetry is considerably lower in energy than the *C*2/*m* phase by a ΔE of 166 and 110 meV per f.u. for SNON and STON, respectively. Regarding the *Pma*2 phase, although it is not the ground state under strain, in the SNON case, it is lower in energy by ΔE of 20 meV per f.u. concerning the non-polar *C*2/*m*. This finding suggests the possible appearance of an additional out-of-plane reversible polarization in the thin-films case.

To better understand the polar displacements, we also extracted the Born effective charges in the *cis*-configuration, as summarized in Table 1. We observed significant charge deviations from the nominal charges when the Z^*_{yy} is analyzed for Nb and Ta, as B-sites, and N and O, as X-sites. As discussed previously for the *trans*-type anionic ordering, these dynamical charge values are in complete agreement with the covalent-driven origin mechanism of the ferroelectric behavior in this 4d, and 5d transition metals with a 5+ oxidation.[67] Interestingly, the Z^* values for Sr in both $SrNbO_2N$ and $SrTaO_2N$ cases are close to their nominal values, although the polar eigendisplacements in the $Pmc2_1$ phases display a clear Sr contribution, as depicted in Fig. 3b. These A-site contributions were also extracted from the eigendisplacements computed in the phonon-dispersion curves in Fig. 2d and e. Therefore, we conclude that in the *cis*-type anionic ordering, on top of the B-site ferroelectricity, which is based on the (Nb,Ta):d-(O,N):p hybridization, a dominating A-site geometrically-driven contribution is demonstrated thanks to the study of the Born effective charges and phonon-dispersion analysis. Then, these findings explain the ferroelectric response and the breaking of symmetry along this *y*-axis.

As performed in the *trans*-type case, we have estimated the ferroelectric spontaneous polarization value for both SNON and STON oxynitrides in the *cis*-type anionic ordering. Here, we found values of P_s = 26.5 μC cm^{-2} and 13.0 μC cm^{-2} for $SrNbO_2N$ and $SrTaO_2N$ respectively under strain where the polar structure is lower in energy and therefore, the structural ground state. Remarkably, we believe that although several anionic combinations could be achieved experimentally, these two mechanisms explained in the *trans*- and *cis*-type anionic orderings, can lead to the reversible polar behavior observed in thin-films. The latter combination of phases is made, in a minor contribution from the *trans*-type ordering compared to the significant contribution from the *cis*-type configuration. This difference in the contribution is following the structural total energy criteria and the experimental findings.[69] Moreover, according to our results, the substrate compressing strain plays a crucial role in the *cis* and *trans* anionic ordering emergence in the oxynitride samples. Then, several properties, such as the switching path, polarization's intensity, and ferroelectric's mechanism, are directly affected by these anionic arrangements. Therefore, we could conclude that the polar response in these oxynitride perovskite compounds is observed as a consequence of the average of the properties shown by different anionic orderings into the samples, rather than the properties of the averaged long-range structure, which, in agreement with the experimental findings, belongs to the non-polar *I*4/*mcm* space group. Moreover, further experimentally and theoretically focused efforts can be combined to explore the effect of specific substrates and interfacial forces in the polar response of these oxynitride perovskite-like materials.

4 Conclusions

The structural, vibrational, and ferroelectric properties of oxynitrides $SrNbO_2N$ and $SrTaO_2N$ are reported. This study was based on first-principles calculations within the density-functional theory framework. Using the site-occupation disorder approach and considering the experimentally reported *I*4/*mcm* reference, we have found an ensemble of nonequivalent structures by symmetry and performed the energetic analysis of each. We found that the lower energy structure belongs to the *cis*-type anionic ordering configuration maximizing the (Nb,Ta):d-N:p overlapping. Nevertheless, a complete characterization of the potential energy surface structures was obtained to clarify the role of the various competitive interactions between the transition metal and N and/or O sites. When analyzing the vibrational landscape, we found that in the *trans*-type configuration, the appearance of a polar-mode drives the out-of-plane ferroelectric response leading the original structure towards an *I*4*cm* ground state in the considered oxynitrides. A ferroelectric

response is also observed in the *cis*-type anionic ordering structure when the in-plane epitaxial strain is considered. Thus, the reversible polarization state belongs to a metastable structure in unconstrained oxynitrides. These structures can be stabilized as the lower energy ground state phases when epitaxial strain is applied. Remarkably, such spontaneous polarization is considerably enhanced by the epitaxial strain, as observed previously in other oxides and thin-films.[70]

In the *trans*-type configuration, the ferroelectric behavior responds to a purely covalent-driven B-site off-centering origin. In contrast, the *cis*-type involves a Sr-sites contribution with geometrically-driven eigendisplacements accompanied by octahedral rotations and (Nb,Ta)-sites off-centering. The latter findings are additionally confirmed by the extracted eigendisplacements and the computed Born effective charges in both cases. We thus hope that this study will clarify the experimental observation of reversible polarization demonstrated in $SrNbO_2N$ and $SrTaO_2N$ oxynitrides in thin films. Moreover, these results will help experimentalists and theoreticians analyze and design novel multifunctional materials based on anionic engineering.

Conflicts of interest

There are no conflicts to declare.

Acknowledgements

Calculations presented in this work were carried out using the GridUIS-2 experimental testbed, being developed under the Universidad Industrial de Santander (SC3-UIS) High Performance and Scientific Computing Centre, development action with support from UIS Vicerrectoría de Investigación y Extensión (VIE-UIS) and several UIS research groups as well as other funding resources. Additionally, we acknowledge the XSEDE facilities' support, a project from the National Science Foundation under grant number ACI-1053575. The authors also acknowledge the Texas Advanced Computer Center (with the Stampede2 and Bridges-2 supercomputers). We also acknowledge the use of the SuperComputing System (Thorny Flat) at WVU, which is funded in part by the National Science Foundation (NSF) Major Research Instrumentation Program (MRI) Award #1726534. ACGC acknowledge the grant no. 2677 entitled "Quiralidad y Ordenamiento Magnético en Sistemas Cristalinos: Estudio Teórico desde Primeros Principios" supported by the VIE – UIS. AHR acknowledges the support of from the National Science Foundation (NSF) under projects 1434897 and OAC-1740111.

Notes and references

1 Y. L. Huang, D. Nikonov, C. Addiego, R. V. Chopdekar, B. Prasad, L. Zhang, J. Chatterjee, H. J. Liu, A. Farhan, Y. H. Chu, M. Yang, M. Ramesh, Z. Q. Qiu, B. D. Huey, C. C. Lin, T. Gosavi, J. Íñiguez, J. Bokor, X. Pan, I. Young, L. W. Martin and R. Ramesh, *Nat. Commun.*, 2020, **11**, 2836.
2 N. A. Spaldin, *Proc. R. Soc. A*, 2020, **476**, 20190542.
3 M. Fiebig, T. Lottermoser, D. Meier and M. Trassin, *Nat. Rev. Mater.*, 2016, **1**, 16046.
4 X. Chai, J. Jiang, Q. Zhang, X. Hou, F. Meng, J. Wang, L. Gu, D. W. Zhang and A. Q. Jiang, *Nat. Commun.*, 2020, **11**, 2811.
5 S. Kim, N. T. Nguyen and C. W. Bark, *Appl. Sci.*, 2018, **8**, 1526.
6 L. Ju, J. Shang, X. Tang and L. Kou, *J. Am. Chem. Soc.*, 2020, **142**, 1492–1500.
7 A. Kakekhani and S. Ismail-Beigi, *J. Mater. Chem. A*, 2016, **4**, 5235–5246.
8 M. Ahmed and G. Xinxin, *Inorg. Chem. Front.*, 2016, **3**, 578–590.
9 D. J. Singh, M. Ghita, M. Fornari and S. V. Halilov, *Ferroelectrics*, 2006, **338**, 73–79.
10 A. C. Garcia-Castro, N. A. Spaldin, A. H. Romero and E. Bousquet, *Phys. Rev. B: Condens. Matter Mater. Phys.*, 2014, **89**, 104107.
11 A. C. Garcia-Castro, A. H. Romero and E. Bousquet, *Phys. Rev. Lett.*, 2016, **116**, 117202.
12 M. Yang, K. C. Amit, A. C. Garcia-Castro, P. Borisov, E. Bousquet, D. Lederman, A. H. Romero and C. Cen, *Sci. Rep.*, 2017, **7**, 7182.
13 A. C. Garcia-Castro, W. Ibarra-Hernandez, E. Bousquet and A. H. Romero, *Phys. Rev. Lett.*, 2018, **121**, 117601.
14 A. C. Garcia-Castro, P. Ghosez, E. Bousquet and A. H. Romero, *Phys. Rev. B*, 2020, **102**, 235140.
15 H. Wang, G. Gou and J. Li, *Nano Energy*, 2016, **22**, 507–513.
16 R. Sarmiento-Pérez, T. F. Cerqueira, S. Körbel, S. Botti and M. A. Marques, *Chem. Mater.*, 2015, **27**, 5957–5963.
17 Y.-W. Fang, C. A. J. Fisher, A. Kuwabara, X.-W. Shen, T. Ogawa, H. Moriwake, R. Huang and C.-G. Duan, *Phys. Rev. B*, 2017, **95**, 014111.
18 K. R. Talley, C. L. Perkins, D. R. Diercks, G. L. Brennecka and A. Zakutayev, Synthesis of ferroelectric $LaWN_3$ – the first nitride perovskite, 2020.
19 S. Bandyopadhyay, A. Paul and I. Dasgupta, *Phys. Rev. B*, 2020, **101**, 014109.
20 J. K. Harada, N. Charles, K. R. Poeppelmeier and J. M. Rondinelli, *Adv. Mater.*, 2019, **31**, 1805295.
21 H. Kageyama, K. Hayashi, K. Maeda, J. P. Attfield, Z. Hiroi, J. M. Rondinelli and K. R. Poeppelmeier, *Nat. Commun.*, 2018, **9**, 772.
22 A. Fuertes, *Mater. Horiz.*, 2015, **2**, 453–461.
23 S. Kikkawa, S. Sun, Y. Masubuchi, Y. Nagamine and T. Shibahara, *Chem. Mater.*, 2016, **28**, 1312–1317.
24 R. Kikuchi, T. Nakamura, S. Tamura, Y. Kaneko and K. Hato, *Chem. Mater.*, 2017, **29**, 7697–7703.
25 D. Oka, Y. Hirose, M. Kaneko, S. Nakao, T. Fukumura, K. Yamashita and T. Hasegawa, *ACS Appl. Mater. Interfaces*, 2018, **10**, 35008–35015.
26 C. Le Paven, R. Benzerga, A. Ferri, D. Fasquelle, V. Laur, L. Le Gendre, F. Marlec, F. Tessier, F. Cheviré, R. Desfeux, S. Saitzek, X. Castel and A. Sharaiha, *Mater. Res. Bull.*, 2017, **96**, 126–132.
27 A. Hosono, Y. Masubuchi, S. Yasui, M. Takesada, T. Endo, M. Higuchi, M. Itoh and S. Kikkawa, *Inorg. Chem.*, 2019, **58**, 16752–16760.

28 D. Oka, Y. Hirose, H. Kamisaka, T. Fukumura, K. Sasa, S. Ishii, H. Matsuzaki, Y. Sato, Y. Ikuhara and T. Hasegawa, *Sci. Rep.*, 2014, **4**, 4987.
29 R. Vadapoo, M. Ahart, M. Somayazulu, N. Holtgrewe, Y. Meng, Z. Konopkova, R. J. Hemley and R. E. Cohen, *Phys. Rev. B*, 2017, **95**, 214120.
30 A. C. Garcia-Castro, Y. Ma, Z. Romestan, E. Bousquet, C. Cen and Aldo H. Romero, 2021, to be Submitted.
31 P. Hohenberg and W. Kohn, *Phys. Rev.*, 1964, **136**, B864–B871.
32 W. Kohn and L. J. Sham, *Phys. Rev.*, 1965, **140**, A1133–A1138.
33 G. Kresse and J. Furthmüller, *Phys. Rev. B: Condens. Matter Mater. Phys.*, 1996, **54**, 11169–11186.
34 G. Kresse and D. Joubert, *Phys. Rev. B: Condens. Matter Mater. Phys.*, 1999, **59**, 1758–1775.
35 P. E. Blöchl, *Phys. Rev. B: Condens. Matter Mater. Phys.*, 1994, **50**, 17953–17979.
36 J. P. Perdew, A. Ruzsinszky, G. I. Csonka, O. A. Vydrov, G. E. Scuseria, L. A. Constantin, X. Zhou and K. Burke, *Phys. Rev. Lett.*, 2008, **100**, 136406.
37 A. I. Liechtenstein, V. I. Anisimov and J. Zaanen, *Phys. Rev. B: Condens. Matter Mater. Phys.*, 1995, **52**, R5467–R5470.
38 H. J. Monkhorst and J. D. Pack, *Phys. Rev. B: Solid State*, 1976, **13**, 5188–5192.
39 X. Gonze and C. Lee, *Phys. Rev. B: Condens. Matter Mater. Phys.*, 1997, **55**, 10355–10368.
40 A. Togo and I. Tanaka, *Scr. Mater.*, 2015, **108**, 1–5.
41 K. Momma and F. Izumi, *J. Appl. Crystallogr.*, 2011, **44**, 1272–1276.
42 D. Vanderbilt, *J. Phys. Chem. Solids*, 2000, **61**, 147–151.
43 R. Grau-Crespo, S. Hamad, C. R. A. Catlow and N. H. de Leeuw, *J. Phys.: Condens. Matter*, 2007, **19**, 256201.
44 C. Giacovazzo, *Symmetry in crystals*, Oxford University Press, Oxford, 3rd edn, 2011.
45 S. G. Ebbinghaus, A. Weidenkaff, A. Rachel and A. Reller, *Acta Crystallogr., Sect. C: Cryst. Struct. Commun.*, 2004, **60**, 91–93.
46 Y.-I. Kim, P. M. Woodward, K. Z. Baba-Kishi and C. W. Tai, *Chem. Mater.*, 2004, **16**, 1267–1276.
47 A. M. Glazer, *Acta Crystallogr., Sect. B: Struct. Crystallogr. Cryst. Chem.*, 1972, **28**, 3384–3392.
48 N. Charles, R. J. Saballos and J. M. Rondinelli, *Chem. Mater.*, 2018, **30**, 3528–3537.
49 N. Charles and J. M. Rondinelli, *Phys. Rev. B*, 2016, **94**, 174108.
50 D. G. Schlom, L.-Q. Chen, C.-B. Eom, K. M. Rabe, S. K. Streiffer and J.-M. Triscone, *Annu. Rev. Mater. Res.*, 2007, **37**, 589–626.
51 D. G. Schlom, L.-Q. Chen, C. J. Fennie, V. Gopalan, D. A. Muller, X. Pan, R. Ramesh and R. Uecker, *MRS Bull.*, 2014, **39**, 118–130.
52 J. Hwang, Z. Feng, N. Charles, X. R. Wang, D. Lee, K. A. Stoerzinger, S. Muy, R. R. Rao, D. Lee, R. Jacobs, D. Morgan and Y. Shao-Horn, *Mater. Today*, 2019, **31**, 100–118.
53 M. Yang, J. Oró-Solée, J. A. Rodgers, A. B. Jorge, A. Fuertes and J. P. Attfield, *Nat. Chem.*, 2011, **3**, 47–52.
54 G. Gou, M. Zhao, J. Shi, J. K. Harada and J. M. Rondinelli, *Chem. Mater.*, 2020, **32**, 2815–2823.
55 K. Page, M. W. Stoltzfus, Y.-I. Kim, T. Proffen, P. M. Woodward, A. K. Cheetham and R. Seshadri, *Chem. Mater.*, 2007, **19**, 4037–4042.
56 N. Vonrüti and U. Aschauer, *Phys. Rev. Lett.*, 2018, **120**, 046001.
57 B. B. Van Aken, T. T. M. Palstra, A. Filippetti and N. A. Spaldin, *Nat. Mater.*, 2004, **3**, 164–170.
58 M. Cruz, D. Valdespino, J. Gervacio, M. Herrera, D. Bueno-Baques, A. Durán, J. Muñoz, A. García-Castro, F. Espinoza-Beltrán, M. Curiel and J. Siqueiros, *Mater. Lett.*, 2014, **114**, 148–151.
59 H. D. Megaw, *Acta Crystallogr.*, 1952, **5**, 739–749.
60 K. Tkacz-Śmiech, A. Koleżyński and W. S. Ptak, *Ferroelectrics*, 2000, **237**, 57–64.
61 R. Cohen, *J. Phys. Chem. Solids*, 2000, **61**, 139–146.
62 D. Vanderbilt, *Curr. Opin. Solid State Mater. Sci.*, 1997, **2**, 701–705.
63 E. Bousquet, M. Dawber, N. Stucki, C. Lichtensteiger, P. Hermet, S. Gariglio, J.-M. Triscone and P. Ghosez, *Nature*, 2008, **452**, 732–737.
64 N. A. Benedek, J. M. Rondinelli, H. Djani, P. Ghosez and P. Lightfoot, *Dalton Trans.*, 2015, **54**, 10543–10558.
65 M. Tyunina, J. Narkilahti, M. Plekh, R. Oja, R. M. Nieminen, A. Dejneka and V. Trepakov, *Phys. Rev. Lett.*, 2010, **104**, 227601.
66 P. Ghosez, X. Gonze and J.-P. Michenaud, *Ferroelectrics*, 1997, **194**, 39–54.
67 P. Ghosez, J.-P. Michenaud and X. Gonze, *Phys. Rev. B: Condens. Matter Mater. Phys.*, 1998, **58**, 6224–6240.
68 A. V. Postnikov, T. Neumann, G. Borstel and M. Methfessel, *Phys. Rev. B: Condens. Matter Mater. Phys.*, 1993, **48**, 5910–5918.
69 Y. R. Zhang, T. Motohashi, Y. Masubuchi and S. Kikkawa, *J. Ceram. Soc. Jpn.*, 2011, **119**, 581–586.
70 C. Ederer and N. A. Spaldin, *Phys. Rev. Lett.*, 2005, **95**, 257601.

